SDM-TDM Reception Based on MIMO Carrier Phase Recovery Technique for Scalable SDM Transmission

Kohki Shibahara[1], Megumi Hoshi[1], and Yutaka Miyamoto[1]
[1]NTT Network Innovation Laboratories, 1-1 Hikari-no-oka, Yokosuka, Kanagawa, Japan
kouki.shibahara.nv@hco.ntt.co.jp

Abstract: We propose MIMO carrier phase recovery (CPR) scheme and its application into SDM-TDM reception. The use of MIMO-CPR with SDM-TDM reception simplifies local oscillator input architecture, hence enabling three-mode-multiplexed 4600-km transmission with single coherent receiver. © 2021 The Author(s)

1. Introduction

Increasing a multiplexing degree on multiple cores/modes over an optical fiber is a promising approach to dramatically enhance transmission capacity for future scalable space division multiplexing (SDM) transport systems. To date, mode-multiplexed transmission experiments with a spatial mode count of 45 in multimode fiber (MMF) and 120 in multi-core (MC) multimode fiber were reported in [1] and [2], respectively. One important issue for boosting SDM transport systems toward future deployment is relaxing a hardware requirement on at transmitters and receivers, which is supposed to scale with the increased number of spatial channels. To this end, we proposed Kalman filter based multiple-input multiple-output (MIMO) structured digital signal processing (DSP) technique in [3] that optimally estimates and removes multiple phase errors observed in coherent SDM detection in a minimum mean square error (MMSE) sense. This technique, referred to as MIMO carrier phase recovery (MIMO-CPR), was experimentally shown to provide simultaneous estimation of multiple phase errors, hence allowing an employment free-running phase-unlocked local oscillator lasers at SDM receivers in a back-to-back and three-mode 51.2-km transmission.

In this work, we present an extended version of MIMO-CPR technique to track vector-valued (i.e. multiple) phase errors in phase-asynchronous SDM systems that works even with multiple-input single-output (MISO) detection regime. Numerical analysis shows that phase tracking performance is improved in accordance with the number of available received signals. We also propose to apply MIMO-CPR technique into a SDM signal reception in conjunction with time division multiplexing (TDM) technique [4], demonstrating a long-haul three-mode transmission over 4608 km using single coherent receiver even with a phase-unlocked local oscillator (LO) laser.

2. MIMO Carrier Phase Recovery (MIMO-CPR)

We consider a SDM system where N_t data streams are transmitted over an SDM link, and also assume to extract d signals out of N_r received signals. For simplicity, signals to be detected are sorted in ascending order: $\{1, \cdots, d\}$. Each light source either in transmitters and receivers are assumed to be operated in a free-running manner, hence phase errors originated from these light sources have an unsynchronized property, described with independently and identically distributed (i.i.d.) Gaussian random variables. Denoting φ_i^t, φ_i^r, as phase error originated from *i*-th transmitter LD for optical signal generation, phase error from *i*-th receiver LD for coherent detection, respectively, the main objective of MIMO-CPR is to provide a simultaneous estimator for $\boldsymbol{\varphi} \triangleq \left[\varphi_1^t, \cdots, \varphi_d^t, \varphi_1^r, \cdots, \varphi_{N_r}^r\right]^T$ at each sample time k, where T is the transpose operator. An end-to-end signal propagation in linear transmission regime is described by a linear SDM-MIMO model: $\boldsymbol{y} = \boldsymbol{D}_r\boldsymbol{H}\boldsymbol{D}_t\boldsymbol{x} + \boldsymbol{z}$, where $\boldsymbol{x}$, $\boldsymbol{y}$, $\boldsymbol{H}$, $\boldsymbol{z}$, $\boldsymbol{D}_t \triangleq \mathrm{diag}\left[e^{j\varphi_1^t}, \cdots, e^{j\varphi_d^t}\right]$, $\boldsymbol{D}_r \triangleq \mathrm{diag}\left[e^{j\varphi_1^r}, \cdots, e^{j\varphi_{N_r}^r}\right]$ are a transmit signal vector, a received signal vector, a channel transfer matrix, a noise vector, a transmitter-side phase-error matrix, and a receiver-side phase error-matrix, respectively. Based on the framework of the extended Kalman filter, the facts that the process equation for $\boldsymbol{\varphi}$ follows the Wiener process [5] and that the measurement equation for output signals from MIMO-DSP are described as $\hat{\boldsymbol{x}} \triangleq \hat{\boldsymbol{D}}_t^H \boldsymbol{W}^H \hat{\boldsymbol{D}}_r^H = \boldsymbol{x} + \tilde{\boldsymbol{z}}$, where $\boldsymbol{W}$, $\tilde{\boldsymbol{z}}$, and H respectively denote the weight matrix of MIMO equalizer, the net noise vector, and the conjugate-transpose operator, lead MIMO-CPR processing as listed in Table 1. In the table, $\boldsymbol{Q}$ and $\boldsymbol{R}$ are covariance matrices of the process noise and the measurement noise, respectively. Processing flow details including the combined use with MIMO equalizer are available in [3]. The main extension in comparison with our previous work [3] is that tracking for multiple phase errors is possible for all regimes of $1 \leq d \leq N_T$: the regime of $d = 1$ corresponds to MISO detection, and that of $d \geq 2$ to MIMO detection.

The performance of the MIMO-CPR technique is analyzed with a numerical back-to-back simulation where 3×3 16-QAM signals generated/received by free-running light sources with a sum linewidth symbol duration product of 5×10^{-5} (corresponding to 10-Baud signals with 250-kHz linewidth lasers) are mutually coupled by a random unitary matrix, and then processed with MIMO-CPR. Figure 1 shows obtained BER curves when the number of detected signals d was changed in the range of $d = \{1, 2, 3\}$. It is obvious that the BER performance outperformed in the case with higher d. Intuitive explanation for this is that the accuracy for tracking $\{\varphi_1^r, \cdots, \varphi_{N_r}^r\}$, which are common phases for all transmitted signal streams, was improved with the increase of supervised learning parameters. The cost is the rather enhanced computational complexity arising from the expansion of the MIMO size [3]. Important consequence of this result is, however, that an estimation of multiple phase errors including $\varphi_1^r, \cdots, \varphi_{N_r}^r$ is possible even in the case of MISO detection (i.e. $d = 1$).

Table 1. MIMO-CPR Algorithm

At each sample time k**, do**
$\hat{\boldsymbol{\varphi}}^-(k) = \hat{\boldsymbol{\varphi}}(k-1)$
$\boldsymbol{P}^-(k) = \boldsymbol{P}(k-1) + \boldsymbol{Q}$
$\hat{\boldsymbol{x}}^-(k) = \hat{\boldsymbol{D}}_t^{-H}(k)\boldsymbol{W}^H(k)\hat{\boldsymbol{D}}_r^{-H}(k)\boldsymbol{y}(k)$
$\boldsymbol{T}(k) = -1j\left[\mathrm{diag}\left(\hat{\boldsymbol{x}}^-(k)\right), \hat{\boldsymbol{D}}_t^{-H}(k)\boldsymbol{W}^H(k)\mathrm{diag}\left(\boldsymbol{y}(k)\right)\hat{\boldsymbol{D}}_r^{-H}(k)\right]$
$\boldsymbol{G}(k) = \boldsymbol{P}^-(k)\boldsymbol{T}^H(k)\left[\boldsymbol{T}(k)\boldsymbol{P}^-(k)\boldsymbol{T}^H(k) + \boldsymbol{R}\right]^{-1}$
$\hat{\boldsymbol{\varphi}}(k) = \hat{\boldsymbol{\varphi}}^-(k) + \boldsymbol{G}(k)\left[\boldsymbol{x}(k) - \boldsymbol{x}^-(k)\right]$
$\boldsymbol{P}(k) = \left[\boldsymbol{I}_{d+N_r} + \boldsymbol{G}(k)\boldsymbol{T}(k)\right]\boldsymbol{P}^-(k)$
$\hat{\boldsymbol{x}}(k) = \hat{\boldsymbol{D}}_t^H(k)\boldsymbol{W}^H(k)\hat{\boldsymbol{D}}_r^H(k)\boldsymbol{y}(k)$

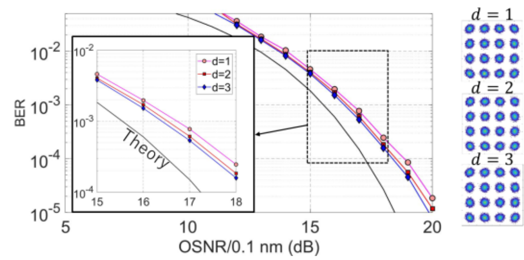

Fig. 1. Averaged BER performance and constellations for 3×3 16-QAM signals obtained by MIMO-CPR in the range of $d = \{1, 2, 3\}$.

3. Experimental Setup for Phase-Asynchronous SDM-TDM Reception

The setup for a long-haul three-mode MDM transmission is shown in Figure 2. The transmission frame comprised a 33360 symbol-length QPSK-pattern containing 25%-overhead (OH) for LDPC decoding defined in DVB-S2 standard and 1.4%-OH for the training sequence. The test channel was generated to be a 12-GBaud PDM-QPSK signal through an IQ-modulator with electrical/optical inputs of a 24-GSa/s AWG and external cavity laser (ECL) with a 25-kHz linewidth, and a PDM emulator with a 295-ns delay for decorrelation. 12.5-GHz-channel-spaced nine signals were also loaded as WDM dummy channels by spectrally shaping ASE source through a wavelength-selective switch [6], located from 1549.627 nm to 1550.529 nm. These signals were combined through a 2×1 optical coupler to yield 10 WDM PDM signals, and then split into three and decorrelated with delays of 0, 566 and 1151 ns for LP_{01} (hereafter denoted as mode 1), LP_{11a} (mode 2), and LP_{11b} (mode 3) inputs, respectively.

To perform long-distance MDM signal transmission, a three-fold recirculating loop system was constructed, each containing mode multiplexer/demultiplexer input/output ports, EDFAs, optical bandpass filters (OBPFs), and AOMs. The transmission fiber was a graded-index FM supporting three modes with a length of 51.2 km, measured DMD of more than 30 ps/km in C band. At the end of the recirculating loop system, we introduced cyclic mode permutation (CMP) technique [7] to equalize mode-dependent transmission properties including mode dispersion and mode dependent loss (MDL). The optical power launched into the FMF was set to -5 dBm/λ/mode.

At the receiver, MDM signals were received through both *SDM receiver* and *SDM-TDM receiver*. For SDM receiver, three-mode MDM signal data was captured simultaneously by three coherent receiver setups in the same manner performed in conventional MDM transmission experiments. On the other hand, when MDM signals were detected through SDM-TDM receiver, the relative delays were introduced for modes 2 and 3 with SMF delay lines of 5 km and 10 km, respectively, and then combined by 3×1 coupler to be properly aligned in the time domain for a reception by a single coherent receiver. In both setup, input power of 25-kHz-linewidth LO into each optical hybrid port was kept as high as 13 dBm. One major difference compared to conventional STM-TDM reception setups as performed in [4] is that a condition of LO phase synchronization between spatial channels was not satisfied in our SDM-TDM reception setup because of the absence of delay lines for the LO input (see Fig.2). We also note that these

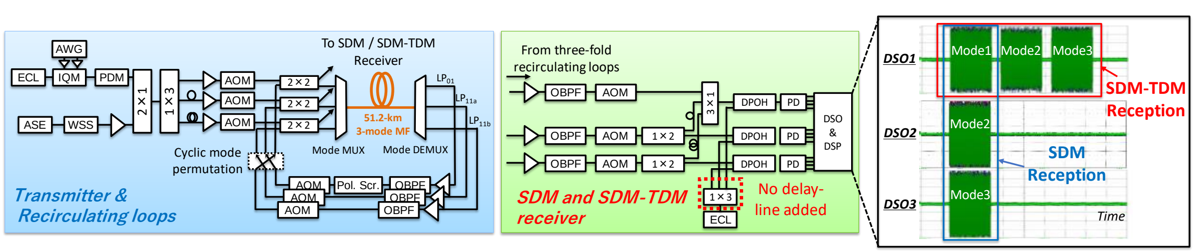

Fig. 2. Experimental setup.

setups enabled us to perform a "fair" comparison of the MDM signal performance between two reception cases (i.e., SDM and SDM-TDM receptions), because these data set were "copies" generated from identical transmitted signals. The detected signals were then stored for an off-line processing, performing front-end error correction, chromatic dispersion compensation, and MIMO equalization in conjunction with proposed MIMO-CPR with $d = 6$. For a comparative purpose we also tested single-input single-output (SISO)-based CPR with identical parameters, which is simply obtained by modifying MIMO-CPR with $d = 1$ and $N_r = 0$.

3. Transmission results

As a preliminary evaluation, we see feasibility of our SDM-TDM reception setup in conjunction with MIMO-CPR technique by comparing a transition from LO-synchronous to asynchronous regimes. To perform this, we temporarily introduced relative delay lines with different length at LO inputs of modes 2 and 3 in a back-to-back configuration. Coherence length calculated from a linewidth value of employed LO lasers was around 1.9 km. Figure 3(a) shows Q-factor transitions as a function of delay line length obtained from equalized 12G-Baud QPSK signals with 9-dB OSNR through SISO-CPR and MIMO-CPR processing. In the results of SISO-CPR, Q-factor performance degraded in receptions with longer delay lines, because couplings between spatial channels impacted as unavoidable inter-mode crosstalk, and cannot be removed. On the contrary, negligible Q-factor variation was observed in equalized signals with MIMO-CPR processing. These results indicate that SDM-TDM reception even with phase-asynchronous LO lasers is expected to be possible by proposed MIMO-CPR technique.

We then perform a long-haul three-mode transmission experiment with SDM and SDM-TDM receivers. Fig. 3(b) and (c) compares phase error evolutions of $\{\varphi_{1X}^r, \varphi_{2X}^r, \varphi_{3X}^r\}$ after 3584-km signal transmission (subscript X denotes the X-polarization). For SDM reception (Fig. 3(b)), estimated phase errors represented almost identical transitions because of a relative delay management within coherence length for LO inputs. Each phase error in SDM-TDM reception (Fig. 3(c)), however, evolved uniquely, indicating that phase-synchronization was not satisfied due to the existence of SMF delays lines into signals of modes 2 and 3. Fig. 3(d) shows Q-factor performance as a function of transmission distance for signals obtained by both receiver setups, together with the estimation results of MDL based on the eigenvalue decomposition of the channel transfer matrix. We confirmed that no bit error after LDPC decoding was not observed with a distance of up to 4608 km, although slight Q-factor deviation between two curves was obtained. This might be due to the penalty of the unsynchronized phase in SDM-TDM reception. To summarize our transmission results, we have succeeded in demonstrating 4608-km three-mode transmission with phase-asynchronous single coherent receiver.

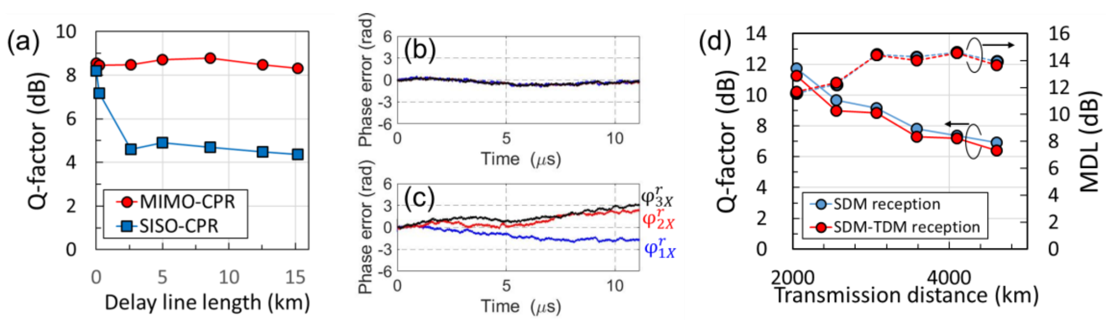

Fig. 3. (a): Q-factor transitions as a function of delay line length obtained by MIMO-CPR (red) and by SISO-CPR (blue). (b): Phase error evolutions of φ_{1X}^r (blue), φ_{2X}^r (red), and φ_{3X}^r (black) in SDM reception. (c): Phase error evolutions with the same figure format of (b) except for those obtained in SDM-TDM reception. (d): Q-factor and MDL transitions as a function of transmission distance in SDM reception (blue) and SDM-TDM reception (red).

4. Conclusion

We have presented a MIMO-CPR technique applicable for phase-asynchronous MIMO-SDM systems. Phase tracking performance is numerically shown to be improved when switching MISO detection to MIMO detection in accordance with the increased number of signals to be detected. We also newly proposed the application of MIMO-CPR scheme to phase-unsynchronized SDM-TDM reception with reduced-count receivers, achieving the 4608-km three-mode transmission with the use of single coherent receiver.

5. References

[1] R. Ryf et al., ECOC2018, Th3B.1 (2018).
[2] T. Sakamoto et al., ECOC2018, We3E.5 (2018).
[3] K. Shibahara et al., Opt. Express, **29**(11), pp. 17111-17124 (2021).
[4] R. Uden et al., Opt. Express, **22**(10), pp. 12668-12677 (2014).
[5] M. Magarini et al., Opt. Express **19**(23), pp.22455-22461 (2011).
[6] T. Richter et al., OFC2018, W1B.2 (2018).
[7] K. Shibahara et al., OFC2018, Th4C.6 (2018).